Aerodynamic Heating Prediction Tool for a Supersonic Vehicle for Conceptual Design Phase

Conference Paper · June 2016

DOI: 10.2514/6.2016-4428

4 authors, including:

Sitki Uslu
TOBB University of Economics and Technology
20 PUBLICATIONS **17** CITATIONS

SEE PROFILE

AIAA Aviation
13-17 June 2016, Washington, D.C.
46th AIAA Thermophysics Conference

Aerodynamic Heating Prediction Tool for a Supersonic Vehicle for Conceptual Design Phase

Buğra ŞİMŞEK[1], Bayındır KURAN[2], Mehmet Ali AK[3]
Roketsan Missiles Industries Inc., Ankara, 06780, Turkey

Sıtkı USLU[4]
TOBB University of Economics and Technology, Ankara, 06560, Turkey

A computational tool has been developed to compute transient surface temperature utilizing basic flight parameters such as altitude, Mach number and angle of attack. An explicit finite difference technique is used to discretize the governing differential equations that account for convection and radiation heat transfer with non-reactive chemistry. Different approaches are applied to two different surface types; thermally thin and thermally thick. The Biot number criterion between the wall and the surrounding air is considered to determine the surface type. Transport properties of air are calculated at Eckert's reference temperature. Boundary layer transition is taken into account by considering local Mach number and Reynolds number. Heat transfer coefficients are calculated by use of flat plate approaches. Effect of angle of attack is taken into account through modified Newtonian theory. The available X-15 flight data for two different flight trajectories and HIFiRE-5 flight data are used to validate the prediction tool. Vehicles with different geometries are modeled using CFD simulations and results of different configurations are compared with the computed temperatures. Predicted results for surface temperatures are found to be in good agreement with measured flight data and simulation results. The validation shows that the methodology developed in the present study could be useful in predicting aerodynamic heating loads during conceptual and preliminary design phases.

Nomenclature

A	=	area
Bi	=	Biot number
c_p	=	specific heat of the structural material
c_{p_flow}	=	specific heat of fluid
C_p	=	pressure coefficient
C_{p_max}	=	maximum pressure coefficient on the body surface
C_m	=	transition Mach number coefficient
E	=	Energy
$\dot{E}_{in}$	=	energy inflow to the structure
$\dot{E}_{out}$	=	energy outflow from the structure
$\dot{E}_{st}$	=	the rate change of thermal energy stored by the structure
h	=	heat transfer coefficient
k	=	thermal conductivity
k*	=	thermal conductivity evaluated at the reference temperature
m	=	mass
M	=	Mach number

[1] Senior Thermal Design Engineer, Roketsan Missiles Industries Inc., bsimsek@roketsan.com.tr
[2] Senior Lead Engineer, Roketsan Missiles Industries Inc.
[3] Manager, Roketsan Missiles Industries Inc.
[4] Asst. Prof., Mechanical Engineering Department, Member AIAA, SusLu@etu.edu.tr

M_L = local Mach number
M_∞ = free stream Mach number
N = number of nodes
Nu = Nusselt number
Nu_x = Nusselt number at a position x.
Re = Reynolds number
Re_L = local Reynolds number
Re_t = local transition Reynolds number
Re_x = Reynolds number at a position x
q = dynamic pressure
Q = rate of heat flow due to aerodynamic heating
P = pressure
P_L = local pressure
P_{0L} = local stagnation pressure
P_∞ = free stream pressure
r = recovery factor
t = time
T = temperature
T_L = local temperature
T_r = recovery temperature
T_{ref} = reference temperature for radiation
T_w = wall temperature
T* = Eckert's reference temperature
U = velocity
x = distance to point of interest from the leading edge/nose tip
α = thermal diffusivity
γ = specific heat ratio of flow
δ = thickness of the structure
ε = emissivity
σ = Stefan-Boltzmann constant
ρ = density
θ = angle normal to freestream
μ = viscosity
Δy = distance between the nodes
Δt = time step size

I. Introduction

At supersonic flight speeds, a detached bow shock wave appears just ahead of a blunt-nosed body. A shock wave is very thin and flow properties can change drastically across it. This wave converts the kinetic energy associated with the flight speed into internal energy of the gas, yielding very high temperatures in the shock layer close to the nose of the body or other stagnation points such as leading edges [1]. In addition, at the downstream of the nose region, viscous dissipation in the boundary layer has dominant effects. In this thin region, the particles of fluid are acted upon by shearing, or viscous, frictional forces and relative velocity between the body and ambient fluid is zero. The kinetic energy of air then appears as heat energy, which causes a temperature rise inside the boundary layer. Some of the heat from the boundary layer flows into the surface of the vehicle. This convective heat transfer called as aerodynamic heating is function of fluid density, body velocity, temperature or enthalpy difference between surface and boundary layer gases and size or sharpness of the moving body[2].

The calculation of the aerodynamic heating is fundamental for supersonic vehicles. It has always been one of the major concerns since the success of the vehicle on target depends on correct evaluation of the thermal loads on the vehicle. Heat transfer calculation of the vehicle structure is required to find the wall temperature to select the material of the structure with suitable wall thickness. In addition, it is required to determine the insulation details and to check design adequacy for ensuring safe operation in the severe thermal environment experienced during flight.

Currently, there are mainly three ways predicting the aerodynamic heating of a vehicle, which are wind tunnel experiments, engineering methods and numerical simulations that solve the Navier-Stokes equations. Wind tunnel

experiments cannot simulate the real environment of flight and are too costly[3]. Elaborated techniques employing CFD poses difficulties such as intense modeling efforts should be allocated and the vast amount of computational time can be spent depending on the element/mesh parameters[4]. Therefore, engineering codes using approximate methods can be used for obtaining rapid estimates with their reasonably accurate results and much less running time compared to multi dimensional numerical simulations. These predictions are used to evaluate the seriousness of the problem and identify the most critical condition for optimization studies in conceptual and preliminary design phases.

In this study a simplified method for calculating the aerodynamic heating on a supersonic vehicle is given. The governing equations account for temperature and heat transfer within the boundary layer as a function of Mach number, altitude and angle of attack. Both laminar and turbulent conditions within the boundary layer are considered. The method given in this study is based upon the "Reference Temperature Method of Eckert". In this approach the heat transfer rates are calculated using the equations developed for incompressible flows with the temperature related parameters evaluated at Eckert's reference temperature[5] which lies somewhere between the wall and the recovery temperature. Lumped heat capacitance method in which temperature gradient along thickness is neglected is used for the thermally thin surfaces. Explicit method including forward difference at any time and a second order central difference for the space derivative are used for the thermally thick surfaces. A modification based on the Mangler transformation is made for the flow passing on conical side of the vehicle[6] and then calculations are continued as for a plat plate. Heat transfer coefficient is iteratively calculated at each time step until convergence is satisfied.

Theoretical background and procedures for calculating the recovery temperature, the reference temperature and the heat transfer coefficients corresponding to both laminar and turbulent flow are presented in the following sections.

II. Mathematical Formulation

A. Governing Equations

A simple 1-dimensional equation under transient conditions with constant properties and no internal generation given in Eq. (1) is solved with explicit time stepping and finite differences in space for the thermally thick walls. Heat transfer equation from the boundary layer to the surface with neglected radiation can be written as given in Eq. (2). This equation is used as boundary condition for the node at the outer surface. Inner surface of the structure is assumed adiabatic. For the calculation of aerodynamic heating, it is necessary to know the heat transfer coefficient and recovery temperature beforehand. However, since it is a function of wall temperature, an iterative calculation is required to find the heat transfer coefficient.

$$\frac{1}{\alpha}\frac{\partial T}{\partial t} = \frac{\partial^2 T}{\partial y^2} \tag{1}$$

$$Q = hA(T_r - T_w) \tag{2}$$

A thermally thin wall can be approximated as one-dimensional heat transfer with nearly uniform internal temperature that increases with time and eventually approaching the recovery temperature. Checking of the assumption that the structure is thermally thin surface is performed by Biot Number condition given in Eq. (3);

$$Bi = h\left[\frac{\delta}{k}\right]_{surface} < 0.1 \tag{3}$$

If the above condition is satisfied, the error associated with using the lumped capacitance method is small. For a thermally thin wall, the first law of thermodynamics is used to determine the unknown temperature of the surface. In this case, relevant terms include heat transfer by convection, radiation from the surface and a change in thermal energy storage. Mathematically, the conservation of energy equation yields:

$$\dot{E}_{st} = \dot{E}_{in} - \dot{E}_{out} \tag{4}$$

Three terms given in Eqn. (4), $\dot{E}_{st}, \dot{E}_{in}$ and $\dot{E}_{out}$ stand for stored heat energy, heat transfer from the boundary layer to surface by convection and radiation heat transfer from the surface to ambient with a reference temperature and these terms can be written as:

$$mc_p \frac{dT}{dt} = hA(T_r - T_w) - \sigma\varepsilon A(T_w^4 - T_{ref}^4) \tag{5}$$

Equation (5) assumes that the adiabatic wall temperature is greater than the insulated wall temperature and wall temperature is greater than the radiation reference temperature. Equation (1) and Eq.(5) are converted to finite difference forms for two different surface types considering lumped capacitance criterion given in Eq. (3) and then iterative solution procedures are started to obtain time dependent temperature histories.

B. Recovery Temperature and Local Flow Conditions

Locations on the vehicle far away from the stagnation point will get most of their heating from the viscous deceleration of the air in the boundary layer. For a high-speed boundary layer, the air is brought to rest at the wall, as a result part of the kinetic energy is converted to heat. Generally, boundary layer is very thin in comparison to the vehicle and large temperature gradient in the boundary layer occurs, especially at the larger Mach numbers[7]. The variable that can be used to estimate the influence of these parameters on the flight conditions is the recovery temperature and mathematically it is expressed as given in Eq. (6).

$$T_r = T_L(1 + r\frac{\gamma-1}{2}M_L^2) \tag{6}$$

The recovery factor must be determined for each flow condition, be it laminar or turbulent. It is commonly defined as $r=\sqrt{\Pr}$ for laminar flow over flat plate and as $r=\sqrt[3]{\Pr}$ for turbulent flow over flat plate[5].

The local Mach number is dependent on local static and stagnation pressure. It can be expressed as given in Eq. (7) by using the inviscid isentropic relations for the values at the surface.

$$M_L = \sqrt{\left[\left(\frac{P_{0L}}{P_L}\right)^{\frac{\gamma-1}{\gamma}} - 1\right]\frac{2}{\gamma-1}} \tag{7}$$

The local stagnation pressure depends on the flow speed. For subsonic range it is calculated using the simple isentropic relations as in Eq. (8). For supersonic range the stagnation pressure is computed by Eq. (9)[7] with the assumption of bow shock behaving similar to a normal shock at the centre in transverse direction.

$$P_{0L} = P_L\left[1 + \frac{\gamma-1}{2}M_\infty^2\right]^{\frac{\gamma}{\gamma-1}} \tag{8}$$

$$P_{0L} = P_{0\infty}\left[\frac{\frac{\gamma+1}{2}M_\infty^2}{1+\frac{\gamma-1}{2}M_\infty^2}\right]^{\frac{\gamma}{\gamma-1}}\left[\frac{2\gamma}{\gamma+1}M_\infty^2 - \frac{\gamma-1}{\gamma+1}\right]^{\frac{1}{1-\gamma}} \tag{9}$$

where

$$P_{0\infty} = P_\infty\left[1 + \frac{\gamma-1}{2}M_\infty^2\right]^{\frac{\gamma}{\gamma-1}} \tag{10}$$

Modified Newtonian theory has been used to predict local surface static pressure. The Newtonian flow concept assumes that upon striking a surface, the freestream flow loses its component of momentum normal to that surface and then moves along the surface with its tangential component of momentum unchanged. By use of this theory local surface pressure is determined from Eq. (11)[7]:

$$P_L = qC_{Pmax}cos^2\theta + P_\infty \tag{11}$$

$$C_{Pmax} = \frac{P_{0L} - P_\infty}{q} \tag{12}$$

Modified Newtonian theory has been shown to be applicable for the prediction of local surface static pressures over all surfaces experiencing non-separated flow[7].The remaining parameter needed to calculate the recovery temperature is the local temperature that is given by Eq. (13).

$$T_L = \frac{T_{0L}}{1 + \frac{\gamma - 1}{2} M_L^2} \tag{13}$$

Free stream pressure, temperature and density are calculated by using U.S Standard Atmosphere, 1976[5] in each time step at corresponding altitude.

C. Heat Transfer Coefficient

In the calculation steps of the heat transfer coefficient, Eckert reference temperature approach is followed. This method is approximate; however, because of its simplicity with reasonable accuracy it is useful for conceptual and preliminary design purposes. In this approach temperature-related transport and thermodynamic properties in the classical incompressible formulae expressions are evaluated at Eckert's reference temperature (T*) which is given in Eq. (14)[5].

$$T^* = T_L + 0.5(T_w - T_L) + 0.22(T_r - T_L) \tag{14}$$

For flow over a flat plate, the Nusselt Number for laminar and turbulent flows as a function of Reynolds and Prandtl numbers are given below respectively[8]:

$$Nu_x = 0.33206\sqrt{Re_x}(Pr)^{\frac{1}{3}} \; ; laminar \; flows \tag{15}$$

$$Nu_x = 0.02914(Re_x)^{\frac{4}{5}}(Pr)^{\frac{1}{3}} \; ; turbulent \; flows \tag{16}$$

where

$$Nu_x = \frac{hx}{k^*} \tag{17}$$

For the points on the conical side, the heat transfer coefficient is multiplied by $\sqrt{3}$ and then calculation is done as for a flat plate[6,9]. For the cone, there is a three-dimensional relieving effect that resulting in thinner boundary layer. This in turn results in larger velocity and temperature gradient in the boundary layer and hence causes a higher heat transfer[9].

D. Laminar to Turbulent Transition Criteria

The transition from laminar to turbulent flow has been the subject of investigation for over 100 years. However, the prediction of boundary layer transition is still more of an art than a science[10]. Two of the primary parameters that affect boundary layer transition are the local Reynolds number and local Mach number[10]. Equation (18) is used to incorporate these parameters to predict transition.

$$logRe_L > (logRe_t + C_m M_L) \tag{18}$$

Based on Eq. (18), if the log of the local Reynolds number at a given point in the trajectory is greater than the log of the local transition Reynolds number plus the transition Mach number coefficient times the local Mach number, the values for the turbulent flows are calculated. Otherwise, laminar flow values are calculated. The user must input the log of the transition Reynolds number and the transition Mach number coefficients. The following table lists the transition Reynolds number and Mach number coefficients recommended[10] and used in the prediction tool.

Table 1. Recommended transition Reynolds number and Mach number coefficients

	$\log Re_t$	C_m
Fuselage	5.5	0.2
Wing- no sweep	5.5	0.2
Wing- with sweep	5.5	0.1

Values given in Table 1 are subject to change if additional information is available, that causes premature transition such as any of the following: surface roughness, shock interaction or flow field contamination[10].

III. Numerical Formulation

For the thermally thick walls, second derivative of Eq.(1) is discretized by using the second-order accurate central difference and time derivative of Eq.(1) is discretized by the first-order accurate forward differencing formula to get Eq.(19). In these numerical equations, i is the grid point at y_0, then the notation i+1 and i-1 refer, respectively, to the grid points at $y_0+\Delta y$ and $y_0-\Delta y$. The time point is represented by n.

$$\frac{T_i^{n+1}-T_i^n}{\Delta t} = \alpha \frac{T_{i-1}^n - 2T_i^n + T_{i+1}^n}{(\Delta y)^2} + O[\Delta t, (\Delta x)^2] \tag{19}$$

Equation (19) is rearranged for all the interior nodes on the structure as;

$$T_i^{n+1} = Fo(T_{i-1}^n) + (1-2Fo)T_i^n + FoT_{i+1}^n \qquad \{n = 0,1,2 \dots ; i = 1,2, \dots \dots, N-1\} \tag{20}$$

In which

$$Fo = \frac{\alpha \Delta t}{(\Delta y)^2} \tag{21}$$

Equation (20) provides an explicit means to calculate temperatures at each node for a future time based on the present temperatures of the nodes.

Convection boundary condition at y=0 is valid in the aerodynamic heating problem. By combining the Eq. (2) with the Fourier's law, Eq.(22) is obtained. The first derivative in Eq.(22) can be discretized by use of central differencing under consideration of fictitious nodes at i=-1. After some rearrangement, it yields Eq. (23) for the temperature of outer boundary node[11].

$$-k\frac{\partial T}{\partial y} + hT_w = hT_r \tag{22}$$

$$T_0^{n+1} = (1-2Fo\beta_0)T_0^n + 2FoT_1^n + 2Fo\gamma_0 \quad \text{for i=0} \tag{23}$$

where

$$\beta_0 = 1 + \frac{\Delta y h}{k} \tag{24}$$

$$\gamma_0 = \frac{\Delta y h}{k} T_r \tag{25}$$

Equation (26) is used for the temperature calculation of the inner most node (i=N) which has adiabatic condition.

$$T_N^{n+1} = 2FoT_{N-1}^n + (1-2Fo)T_N^n \tag{26}$$

In the case of insulated structures, since two different materials are involved, Eq. (20) is solved separately for each node with corresponding material properties. For the node at the interference, a new numerical explicit equation is derived by use of the energy balance method[12].

Explicit method used in the calculations is not unconditionally stable. Under some conditions, solution may be characterized by numerically induced oscillations, which are physically impossible. The oscillations may become unstable, causing the solution to diverge. To prevent such erroneous results, a stability criterion given in Eq. (27) shall be satisfied for the interior nodes[12]. In addition, Eq. (28) shall be satisfied for the exterior node on which aerodynamic heating is applied[12]. In the prediction tool, stability criteria are checked in all of the iterations.

$$Fo \leq \frac{1}{2} \tag{27}$$

$$Fo(1 + Bi) \leq \frac{1}{2} \tag{28}$$

For the thermally thin walls, differential Eq. (5) is discretized as given in Eq. (29).

$$T_{w,i+1} = \left[hA(T_r - T_w) - \sigma\varepsilon(T_w^4 - T_{ref}^4)\right]\frac{\Delta t}{mc_p} + T_{w,i} \tag{29}$$

To ensure the stability and increase the accuracy, time step size is selected as too small. Time step size is 0.00125 seconds and mesh size is less than 0.5 mm in the calculations.

IV. The Prediction Tool Structure

The tool consists of six major sections which are data entry, atmospheric property generation, recovery temperature calculation, heat transfer coefficient calculation, explicit solution for the temperature distribution and data output.

Data entry includes manual input of thickness of the structure and insulation (if exists), material properties, initial temperature and initial atmospheric properties, distance from nosetip and type of shape (conical or planar) of the side and total number of nodes. In addition, flow parameters such as ideal gas constant, specific heat ratio etc., and reading of flight profile from a .txt file which includes time dependent Mach, altitude and angle of attack are entered.

Atmospheric property generation is made by fourth order interpolating the tabulated values of U.S Standard Atmosphere 1976. Free stream temperature, density and pressure values are calculated in this section.

Recovery temperature is calculated at the third section. Required dynamic pressure, velocity of the vehicle, temperature and pressure values at the edge of the boundary layer (local conditions) are calculated by use of atmospheric properties found in the second section of the prediction tool.

In the fourth section heat transfer coefficient is found. Eckert's reference temperature and flow properties at this reference temperature are calculated to find the corresponding Reynolds number. Transition criterion is checked and corresponding heat transfer coefficients are computed.

Temperature values of the nodes are found by use of explicit method in the fifth section. Stability is checked and if the solution encounters instability, warning message is printed on the screen.

Fourth and fifth sections are connected each other to calculate heat transfer coefficient iteratively. Changes on the outer surface temperature, affects the Eckert's reference temperature. Therefore, heat transfer coefficient and temperature values of nodes are calculated until the absolute difference between the two successive calculated heat transfer coefficients is less than 0.001 W/m^2K.

In the last section, all of the input and calculated parameters are printed and temperature history of the nodes, time dependent cold wall heat flux and hot wall heat flux, Biot numbers and heat transfer coefficients are plotted. General flowchart of the prediction tool is given Fig.1.

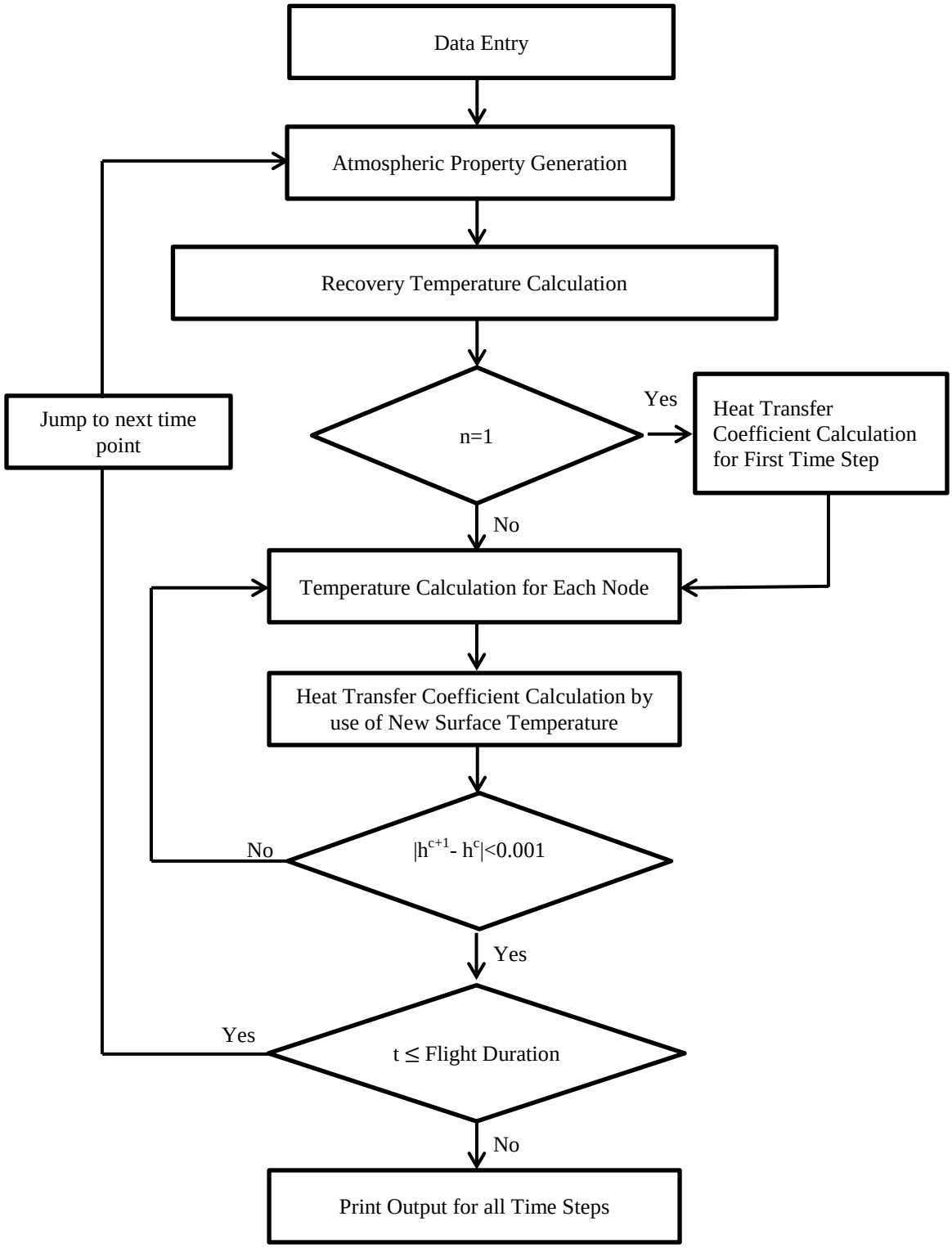

Figure 1. Flowchart of the prediction tool.

V. Validation of the Tool

The validation of the prediction tool is done with results obtained from CFD simulations and test data found in the literature[13,14]. X-15 flight data for 4% chord location at two different flight trajectories and HIFiRE-5 flight data of x=300 mm, are used in the comparisons. CFD simulations are conducted for an axisymmetric generic shape vehicle and comparisons are made for the points on both conical and planar sides.

A. X-15 Test Case

X-15 flight data of two different flight trajectories are used for the validation of the procedure for predicting transient surface temperatures. Location of 4% chord is used in the comparisons. Flight data and material properties are taken from Ref.13. Both windward and leeward sides are taken into account. Comparisons are given in Fig.2 and Fig.3.

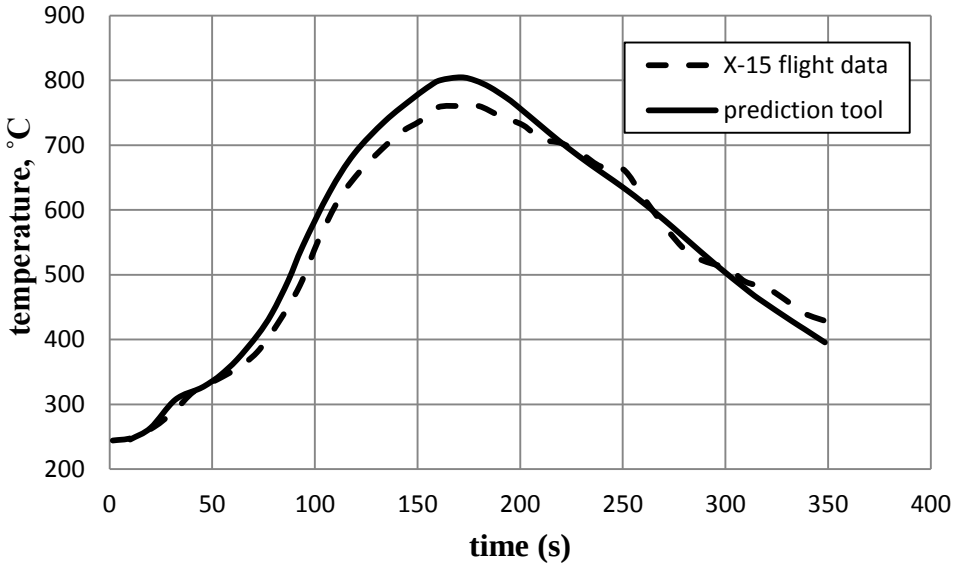

Figure 2. Comparison of measured and computed temperatures of X-15, 4% chord, flight C, windward.

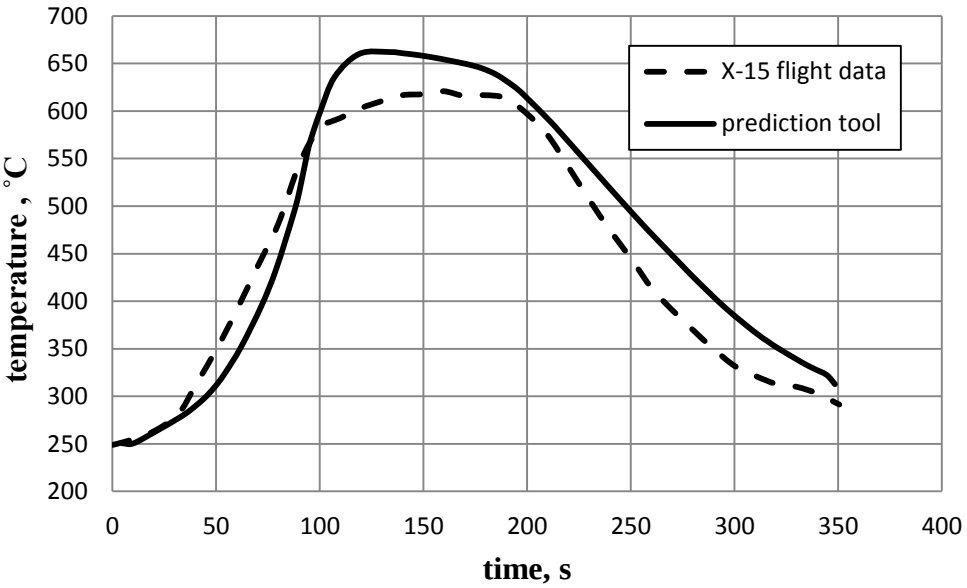

Figure 3. Comparison of measured and computed temperatures of X-15, 4% chord, flight B, leeward.

B. HIFiRE-5 Test Case

HIFiRE-5 is a hypersonic test vehicle designed to examine the aerothermodynamics of a 3-D geometry[14]. Its flight test occurred in 2012, provides a wealth of supersonic aeroheating data[14]. In this study, one of the measured temperature histories is used to validate the prediction tool. Velocity, angle of attack and altitude histories of the vehicle are taken from Ref.14. Prediction is made for the point on the conical side at which x=300 mm. Material of the structure is taken as aluminum as given in Ref.14. Comparison of measured and computed temperatures is given in Fig.4.

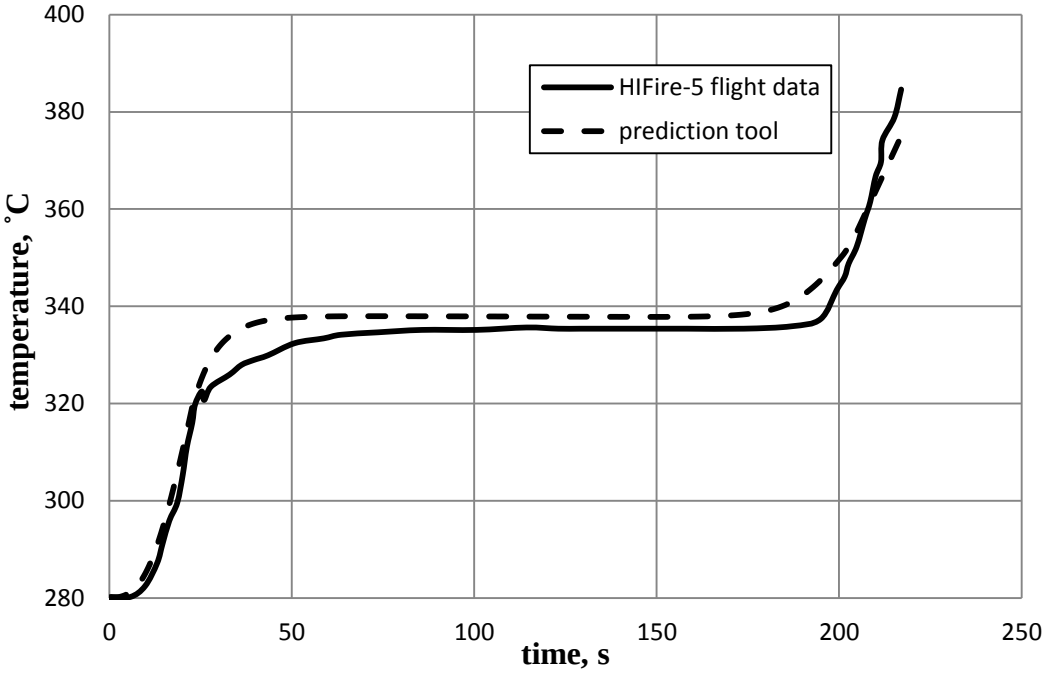

Figure 4. Comparison of measured and computed temperatures for HIFiRE-5, x=300 mm.

C. CFD Simulations

Computed surface temperature histories of four configurations with different parameters are compared with results of simulations made through commercially available CFD simulation software. A generic trajectory for a supersonic vehicle is used in the computations. Temperature histories of two points on conical side, x=500 mm, and planar side, x=1100 mm, of the vehicle are compared. Temperature histories are normalized by dividing the maximum temperature found by simulation or prediction tool to draw attention to the trends and percent differences rather than exact values. Time is normalized by using total flight duration. Configurations used in the simulations are given in Table 2.

Table 2. Configurations used in the simulations.

Configuration	Structural Material	Insulation	Wall Thickness, mm
1	Steel	No	3
2	Steel	No	6
3	Aluminum	No	3
4	Steel	Yes	3

For the uninsulated configurations, only outer surface temperature profiles are given since temperature gradient is too small. For the insulated configuration both of outer and inner surface temperature profiles are given. Comparisons are given in Figures 5-12.

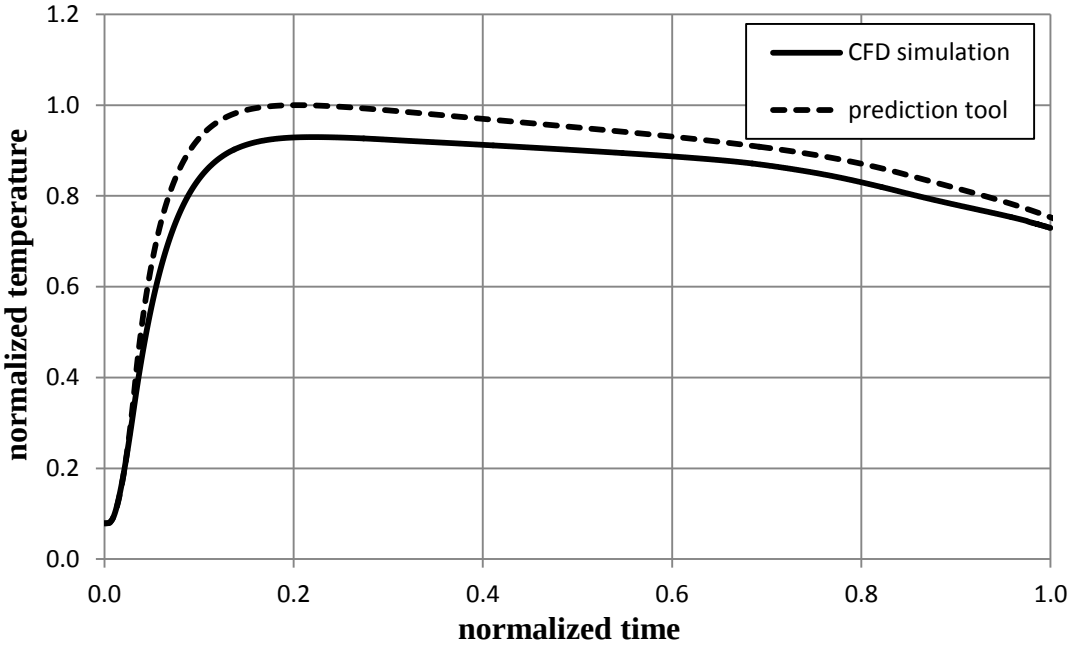

Figure 5. Simulated and computed outer surface temperatures, configuration 1, x=1100 mm.

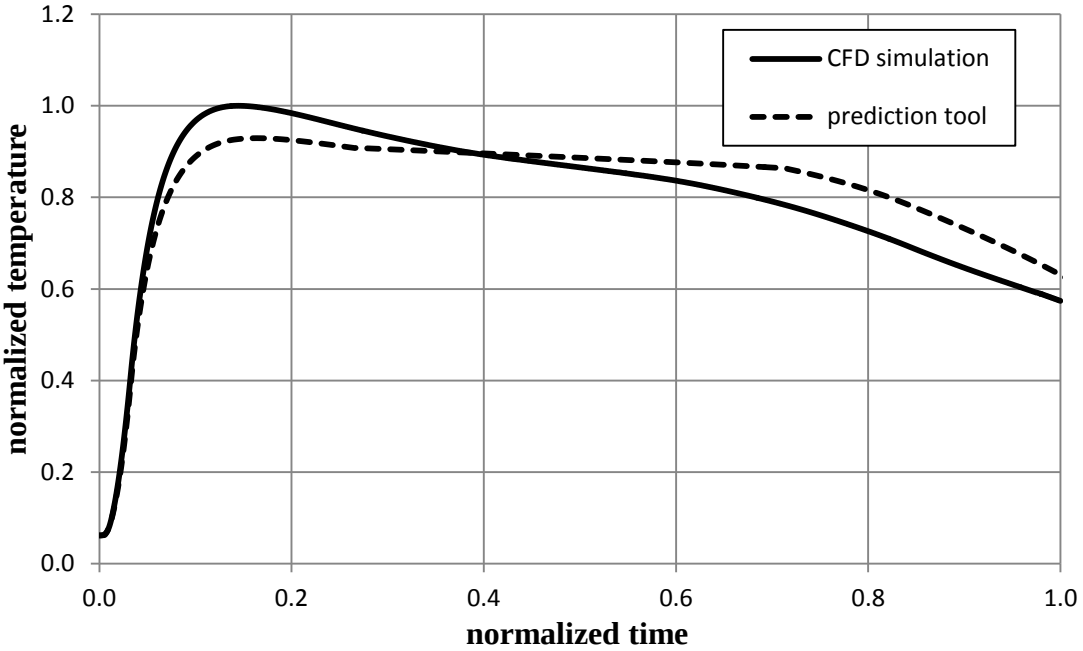

Figure 6. Simulated and computed outer surface temperatures, configuration 1, x=500 mm.

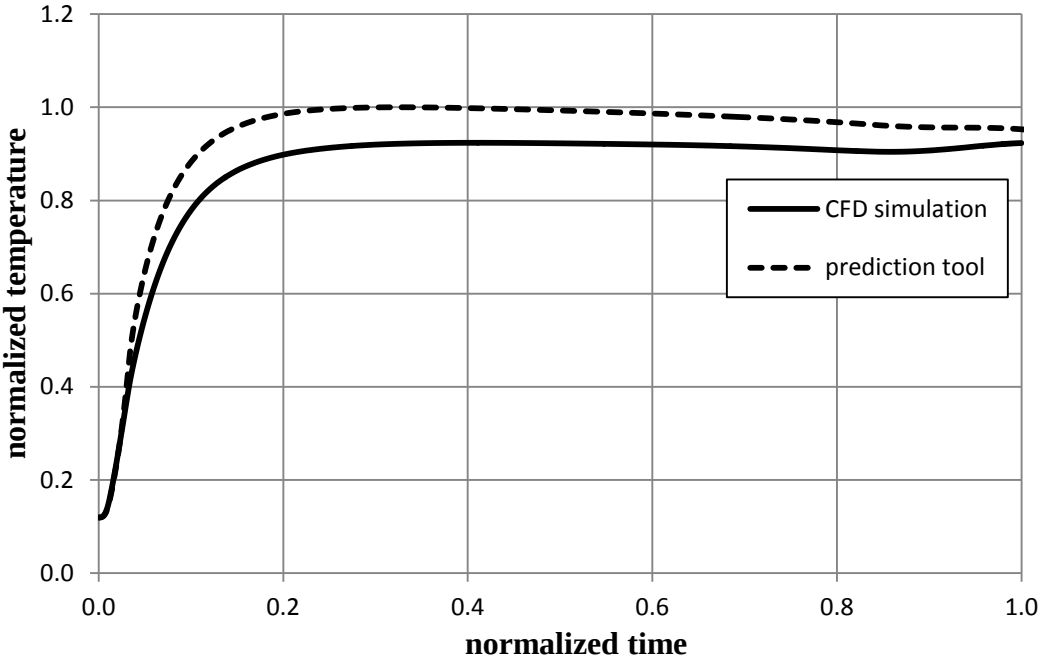

Figure 7. Simulated and computed outer surface temperatures, configuration 2, x=1100 mm.

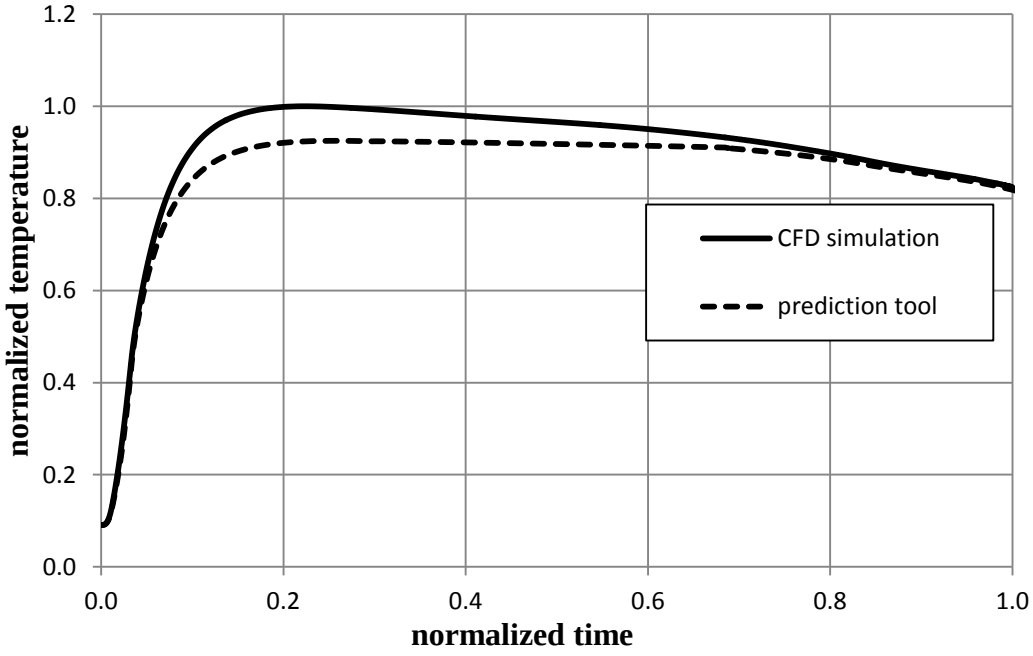

Figure 8. Simulated and computed outer surface temperatures, configuration 2, x=500 mm.

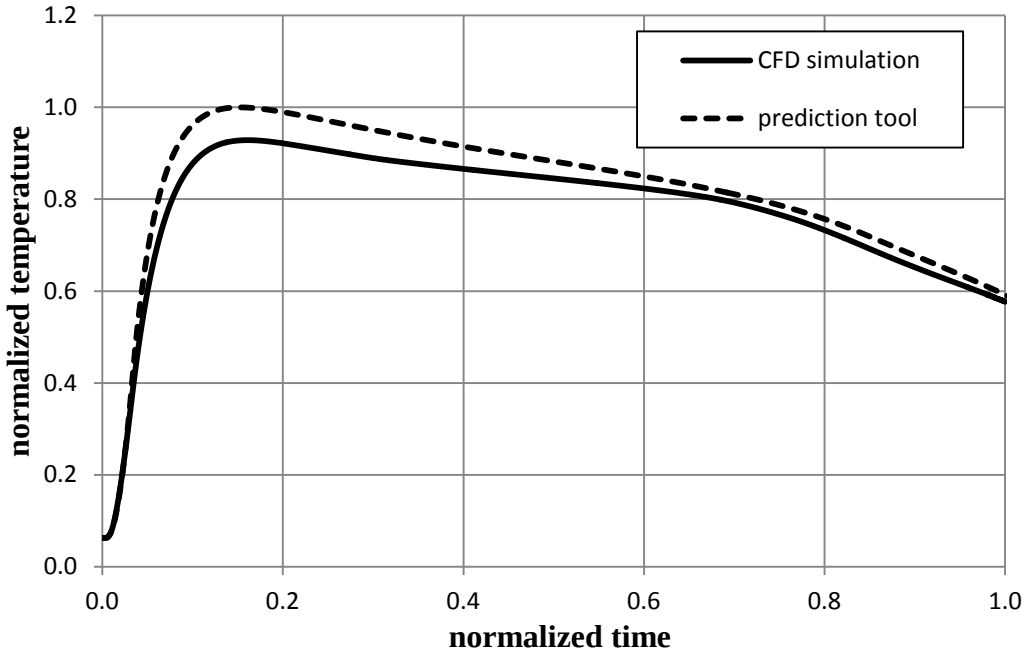

Figure 9. Simulated and computed outer surface temperatures, configuration 3, x=1100 mm.

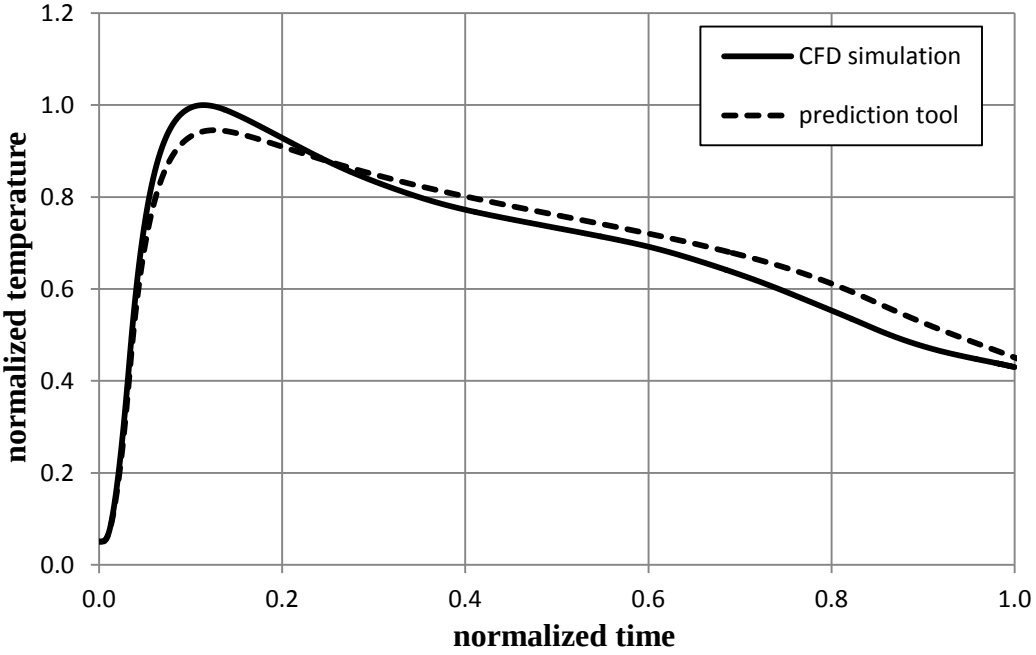

Figure 10. Simulated and computed outer surface temperatures, configuration 3, x=500 mm.

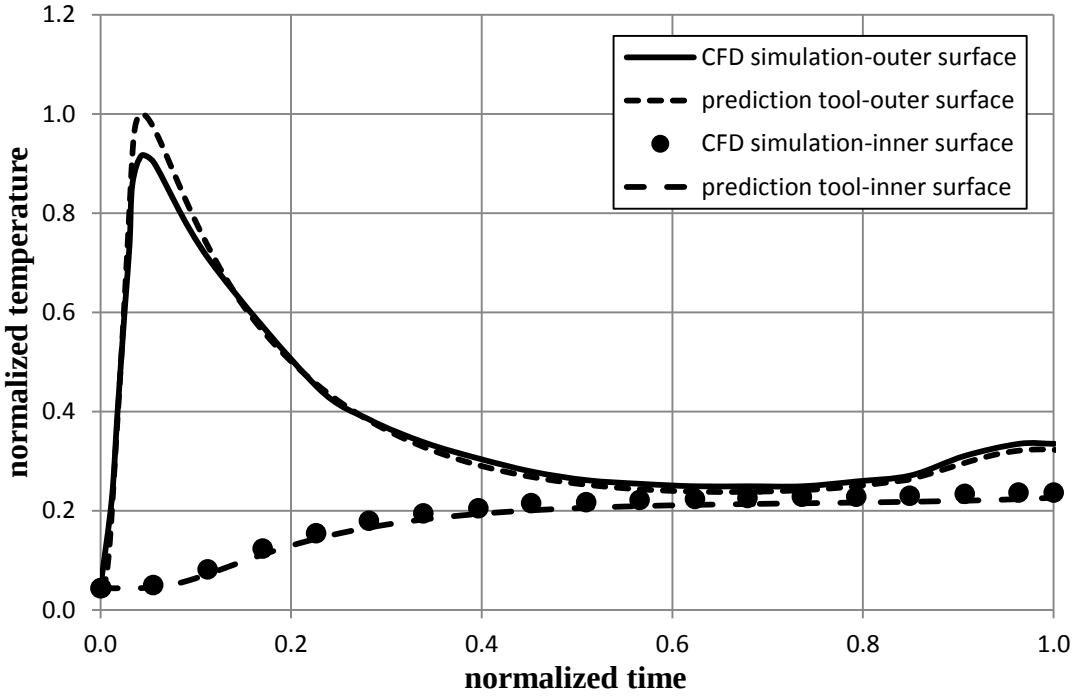

Figure 11. Simulated and computed outer and inner surface temperatures, configuration 4, x=1100 mm.

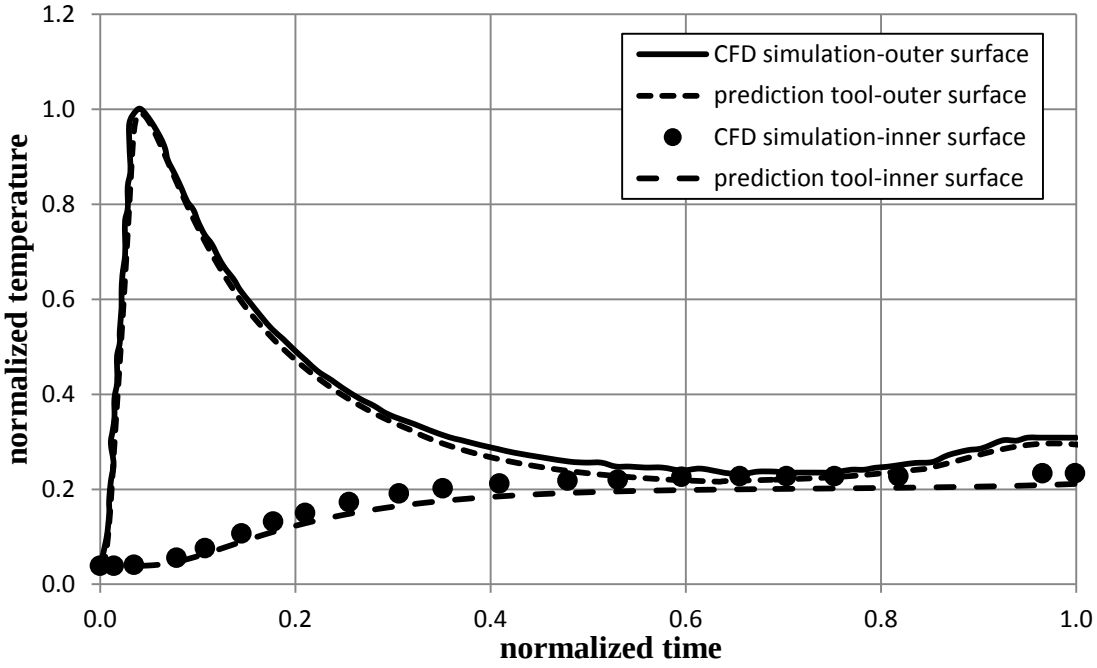

Figure 12. Simulated and computed outer and inner surface temperatures, configuration 4, x=500 mm.

Maximum Biot numbers computed during flight period for each configuration are given in Table 3. An increase in the thickness and heat transfer coefficient yields larger Biot number. The highest Biot numbers are seen in the insulated configuration as expected.

Table 3. Maximum Biot numbers.

Configuration	Location	Max. Biot Number
1	Planar	0.042
	Conical	0.058
2	Planar	0.085
	Conical	0.118
3	Planar	0.015
	Conical	0.017
4	Planar	11.00
	Conical	15.00

VI. Conclusion

An approximate aerodynamic heating prediction tool has been developed for supersonic vehicles and shown to calculate temperatures that compare well to flight data of X-15, HIFiRE-5 and results of CFD simulations. Two different approaches are followed: thermally thin and thermally thick. Thermally thin approach is followed only in the calculations of X-15 data. According to Fig.2 and Fig.3 for the windward side, maximum percent error between the measured and computed temperatures is nearly 5% and for the leeward side maximum percent error is nearly 8%. Using of temperature dependent material properties instead of constant material properties for the structural material and performing the thick wall approach instead of thin wall approach may decrease the errors. Flow separation effects on the leeward side may be the main reason for the higher level of percent error seen in leeward side. Trend of temperature profiles are very similar for each condition. Considering HIFiRE-5 data, comparison of the computed and measured data of thermocouple at x=300 mm is given in Fig.4 and it is seen that maximum difference between the temperatures are less than 10 K. Flight data are used as found in the corresponding references and uncertainties on them may reduce or increase the percent differences seen in the comparisons. Reliability of the flight data is not examined in this study. Comparisons between the prediction tool and CFD simulations were made for four different configurations of a supersonic vehicle. Effects of location, material type, thickness and insulation on the temperature histories are examined and calculated temperature profiles are compared with the results found by CFD simulation. It is seen that for the locations on the planar side of the uninsulated vehicle, tool predicts higher temperatures compared to CFD but maximum error does not exceed 8% in each configuration. General trend of the computed and simulated temperature profiles are very similar. Thinner configurations show fast response to the aerodynamic heating as seen in Fig.5 and Fig.9. Trends in temperature profiles, increasing or decreasing, mainly depend on the surface temperature and recovery temperature. At the time when recovery temperature is higher than surface temperature, structure is heated and temperature goes up, in the opposite case, structure is cooled and temperature goes down. As the structure becomes thicker, slope of the curves decreases due to increase in the thermal inertia as seen in Fig 7. and Fig.8. For the locations on the conical side of the vehicle, maximum errors between the results are smaller than 9% and at some points CFD results are higher than results found by tool. Effects of shock wave generated on the nosetip are more drastic on the boundary layer parameters of the conical side. In the CFD simulations, shock wave effects are taken into the account and this may be the reason of the higher level of temperatures. For the insulated configuration, surface temperature rises rapidly due to low thermal conductivity of the insulation material as seen in both CFD simulations and computations of prediction tool. At the planar side maximum error is less than 8% and at the conical side it is less than 2%. Slope of the temperature profiles for the inner surfaces are very small compared to uninsulated structures. In all of the calculations, absolute values of the maximum temperatures are higher at the conical section since heat transfer coefficient is larger in this side. Considering the Biot numbers given in Table 3, insulated structure has larger values; therefore, temperature gradient in these structures cannot be neglected as in thin wall approach. Biot numbers in the conical sides are larger than that

of planar sides due to increase in the heat transfer coefficients. The smallest Biot numbers are seen in the aluminum structure due to higher thermal conductivity of this material compared to steel.

Simplified heat of ablation model for the ablative type insulation materials will be implemented into the prediction tool in the future works to estimate the surface recession during the flight period.

A prediction tool that determines the transient wall temperatures of supersonic vehicles is developed and validated. Tool can be used over a wide range of trajectories, configurations and it rapidly finds results that enable the user to investigate changes in material characteristics, insulation thickness and flight parameters without having to employ calculations that are more complex.

References

[1]Thornton E.A., Thermal Structures and Materials for High Speed Flight, Progress in Astronautics and Aeronautics, AIAA, Washington, DC, Volume 140, 1992, Chapter 1.

[2]Achard, T.R., "Fundamental Relationships for Ablation and Hyperthermal Heat Transfer", Structure Division of the Air Force Flight Dynamics Lab., Rept. AFFDL-TR-66-25, Wright-Patterson Air Force Base, OH, 1965.

[3]Yang, G., Duan, Y., Liu, C., Cai, J., "Approximate Prediction for Aerodynamic Heating and Design for Leading-edge Bluntness on Hypersonic Vehicles", AIAA 2014-1393,2014.

[4]Simsek, B., Kuran, B., Tunc, T., Yüncü, H., "Thermal Reliability Prediction of External Insulation System in Supersonic Speeds Using Surrogate Models", AIAA 2011-2038, 2011.

[5]Bertin, J.J., *Hypersonic Aerothermodynamics*, AIAA Education Series, AIAA, Washington, 1994, Chaps.1, 7.

[6]Böhrk, H., Dittert, C., Weihs H., Thiele T., Gülhan, A., "Sharp Leading Edge at Hypersonic Flight: Modeling and Flight Measurement", *Journal of Spacecraft and Rockets*, Vol.51, No.5, 2014. pp 1753-1760.

[7]Duarte, G.F.R., Silva, M.G., Castro, B.M., "Aerodynamic Heating Of Missile/Rocket-Conceptual Design Phase", *20th Int. Congress of Mechanical Engineering*, ABCM, Rio De Janeiro, 2009.

[8]Arnas, A. Ö., Daisie, D. B., Gunnar, T., Seth, A.N., Jason, R.W., Michael, J. B., Bret, P. V., "On the Analysis of the Aerodynamic Heating Problem", *Journal of Heat Transfer*, Vol. 132, No.12, 2010.

[9]Anderson Jr., J.D., *Hypersonic and High Temperature Gas Dynamics*, AIAA Education Series, AIAA, Reston,VA,2006, Chapter 6.

[10]Quinn R.D., Gong L., "A Method For Calculating Transient Surface Temperatures And Surface Heating Rates For High-Speed Aircraft", Dryden Flight Research Center, Rept. NASA/TP-2000-209034, Edwards, CA, 2000.

[11]Özışık, M.N., *Finite Difference Methods in Heat Transfer*, CRC Press, Inc., Boca Raton, FL, 1994, Chapter 5.

[12]Bergman,T.L.,Lavine,A.S.,Incropera,F.P.,DeWitt,D.P.,*Fundamentals of Heat and Mass Transfer*,John Wiley&Sons,2006.

[13]Hussain, M., Qureshi M.N., Prediction Of Transient Skin Temperature Of High Speed Vehicles Through CFD, *6th Int. Conference on Recent Advances in Space Technologies*, IEEE, New York, 2013, pp. 723-728.

[14]Juliano, T. J., Adamczak, D., Kimmel, R.L., HIFiRE-5 Flight Test Results, *Journal of Spacecraft and Rockets*, Vol.52, No. 3, 2015, pp.650-662.